Human Molecular Genetics, 2009, Vol. 18, No. 21 **4089–4101**
doi:10.1093/hmg/ddp358
Advance Access published on July 31, 2009

Evaluation of the therapeutic potential of carbonic anhydrase inhibitors in two animal models of dystrophin deficient muscular dystrophy

Jean Giacomotto[1,†], Cordula Pertl[2,†], Caroline Borrel[1], Maggie C. Walter[2], Stefanie Bulst[2], Bob Johnsen[3], David L. Baillie[3], Hanns Lochmüller[4], Christian Thirion[2] and Laurent Ségalat[1,*]

[1]Centre de Génétique Moléculaire et Cellulaire, UMR 5534, Université Lyon 1, 69622 Villeurbanne Cedex, France, [2]Laboratory of Molecular Myology, Department of Neurology, Friedrich Baur Institute, Ludwig Maximilians University of Munich, Munich, Germany, [3]Department of Molecular Biology and Biochemistry, Simon Fraser University, Burnaby, BC, Canada, V5A 1S6 and [4]Institute of Human Genetics, Newcastle University, Newcastle upon Tyne, UK

Received June 8, 2009; Revised July 6, 2009; Accepted July 27, 2009

Duchenne Muscular Dystrophy is an inherited muscle degeneration disease for which there is still no efficient treatment. However, compounds active on the disease may already exist among approved drugs but are difficult to identify in the absence of cellular models. We used the *Caenorhabditis elegans* animal model to screen a collection of 1000 already approved compounds. Two of the most active hits obtained were methazolamide and dichlorphenamide, carbonic anhydrase inhibitors widely used in human therapy. In *C. elegans*, these drugs were shown to interact with CAH-4, a putative carbonic anhydrase. The therapeutic efficacy of these compounds was further validated in long-term experiments on *mdx* mice, the mouse model of Duchenne Muscular Dystrophy. Mice were treated for 120 days with food containing methazolamide or dichlorphenamide at two doses each. *Musculus tibialis anterior* and diaphragm muscles were histologically analyzed and isometric muscle force was measured in *M. extensor digitorum longus*. Both substances increased the tetanic muscle force in the treated *M. extensor digitorum longus* muscle group, dichlorphenamide increased the force significantly by 30%, but both drugs failed to increase resistance of muscle fibres to eccentric contractions. Histological analysis revealed a reduction of centrally nucleated fibers in *M. tibialis anterior* and diaphragm in the treated groups. These studies further demonstrated that a *C. elegans*-based screen coupled with a mouse model validation strategy can lead to the identification of potential pharmacological agents for rare diseases.

INTRODUCTION

Duchenne muscular dystrophy (DMD) is a progressive disorder affecting striated and cardiac muscles. It is caused by mutations in the dystrophin gene (1,2), one of the largest gene in the human genome. This gene encodes a large cytoskeletal protein called dystrophin that links the cytoskeleton to the extracellular matrix (3–5). DMD is the most prevalent X-linked recessive neuromuscular disorder, affecting 1 in 3500 male children.

There is still no curative treatment available against DMD. Current treatments for DMD are symptomatic and significantly improve longevity and quality of life but do little to prevent loss of muscle function (6). The standard care applied to DMD patients is prednisone therapy (7). Several therapeutic strategies have been developed in the past decade for which clinical trials have already been initiated: the reconstitution of dystrophin expression by replacing the mutated gene using adeno associated virus (AAV) vectors (8), repairing the endogenous gene by antisense-mediated

*To whom correspondence should be addressed at: CNRS-CGMC-UMR5534, Universite Lyon-1 Claude Bernard, Batiment Mendel, 43 bld du 11 Novembre, 69622 Villeurbanne Cedex, France. Tel: +33 472432951; Fax: +33 472432951; Email: segalat@cgmc.univ-lyon1.fr
†G.J. and C.P. contributed equally to the study.

exon skipping (9), stop codon readthrough, upregulation of compensating molecules such as utrophin (10), blocking muscle degradation by myostatin inhibition, anti-inflammatory therapy, cell-based therapies (11,12). However, efficacy and safety of those novel therapeutic approaches is still a matter of debate. Consequently, testing small molecules for therapeutic efficacy against DMD is a valuable approach.

Since mice have a high unitary cost, random screens of large numbers of compounds on mouse model may not be feasible. In addition, there is still no *in vitro* model that recapitulates enough properties of the disease. Invertebrate models such as *Caenorhabditis elegans* are complementary models to the mouse because they are cheap, grow rapidly and are amenable to large genetic studies (13–15). So, the main purpose of screens conducted on *C. elegans* is to serve as a first-pass filter, in order to select lead compounds out of chemical libraries, and to eventually test the selected items on the *mdx* mouse.

Caenorhabditis elegans possesses a dystrophin-like gene (*dys-1*) encoding a protein displaying the same structural features as the human dystrophin (16). When in a sensitized *hlh-1* genetic background, *dys-1* mutations lead to a progressive impairment of locomotion (17). Examination of the musculature of these animals reveals a widespread degeneration of the body-wall muscles which are responsible for the animal locomotion. These muscles have a sarcomeric structure and protein composition closely related to mammalian striated muscles (18). However, *C. elegans* striated muscles are different from those of mammals on two aspects: muscle cells do not fuse, and they are not able to regenerate.

Carbonic Anhydrases (CA) are a family of metalloenzymes which have various tissue distributions and intracellular locations in mammals (19–21). There are several cytosolic isoforms (CA I—III, CA VII and CA XIII), five membrane-bound isozymes (CA IV, CA IX, CA XII, CA XIV and CA XV), two mitochondrial forms (CA VA and VB), as well as a secreted CA isozyme, CA VI. These enzymes catalyze the interconversion between carbon dioxide and the bicarbonate ion. They are thus involved in crucial physiological processes connected with respiration and transport of CO_2/bicarbonate between metabolizing tissues and lungs. They are also involved in regulation of pH, CO_2 homeostasis, electrolyte secretion in a variety of tissues/organs, biosynthetic reactions, bone resorption, calcification, tumorigenicity and many other physiologic or pathologic processes (22,23). Since CAs are involved in a large variety of processes, they represent an important therapeutic target. Disorders including oedema, glaucoma, obesity, cancer, epilepsy, osteoporosis, periodic paralysis and ataxia are treated with CA inhibitors (20,21).

A screen of approximately 1000 compounds on the *dys-1(cx18)*, *hlh-1(cc561)* model identified several substances that ameliorated the *C. elegans dys*-deficient phenotype. Two of the top-five hits turned out to be methazolamide (MTZ) and dichlorphenamide (DCPM). These molecules belong to the class of sulfonamides, known inhibitors of CA enzymes. In our study, CA inhibitors were assessed for their therapeutic potential of dystrophin-deficient muscular dystrophy in two animal models, *C. elegans* and the *mdx* mouse.

RESULTS

Effect of MTZ and DCPM on *C. elegans* dystrophin-deficient muscle

We exploited a *C. elegans* model of dystrophin-dependent muscle degeneration in a screen of bioactive molecules to identify potential blockers of muscle degeneration. The relevance of such a screen has been previously demonstrated (24). During this screen, we observed by visual inspection that 7-day *dys-1(cx18)*; *hlh-1(cc561)* adult animals grown on 0.5 mg/ml (2 mM) of MTZ or on 0.1 mg/ml (0.3 mM) of DCPM plates moved better than untreated animals, suggesting that the function of the body wall muscles in these animals was partially conserved. Examination of the musculature by phalloidin staining, which labels actin fibers, revealed a dramatic reduction of muscle degeneration in treated animals (Figs 1 and 2). Whereas the untreated dystrophic animals show 5–6 degenerating or dead muscle cells per pair of quadrants, the animals treated with MTZ or DCPM present only 1–2 such cells.

Dose–response experiments (Fig. 1) showed that the effect of MTZ and DCPM on muscle degeneration is optimal at 0.5 mg/ml and at 0.1 mg/ml in the medium, respectively (Fig. 1). The positive effect was qualitatively visible down to 0.1 mg/ml for MTZ and down to 0.01 mg/ml for DCPM. Concentration of drugs in the medium above 1 mg/ml of MTZ or 0.5 mg/ml of DCPM was toxic to the animals. The actual drug concentration in the animal is not known but is thought to be 100–1000× lower.

The muscle degeneration in the DMD worm model is caused by the synergy between *dys-1(cx18)* and *hlh-1(cc561)* mutations, in which the mild *hlh-1(cc561)* mutation serves as an amplifier of the *dys-1(cx18)* phenotype (17). Therefore, we wanted to verify that MTZ or DCPM were also active on the *dys-1(cx18)* mutation alone. The dose-effect experiments on *dys-1(cx18)* showed a decrease in muscle degeneration similar to that of the double mutant (Fig. 1).

The degeneration observed in the DMD worm model is activity- and time-dependent (17). Consequently, compounds that have a sedative effect or reduce growth rate also reduce muscle degeneration. To verify that MTZ and DCPM did not act this way, but had a real beneficial effect on muscle, we tested their impact on these parameters. Addition of 0.5 mg/ml of MTZ or 0.1 mg/ml of DCPM had no sedative effect on the locomotion and growth rate of *dys-1(cx18)* or wild-type worms compared with untreated animals (Fig. 3A and B). These results demonstrated that the gain obtained with MTZ and DCPM on muscle degeneration is not due to a sedative effect or to a reduced growth rate.

Effect of CA inhibition on *C. elegans* dystrophin-deficient muscle

Since we found that MTZ and DCPM can reduce muscle degradation in the dystrophic model of *C. elegans*, we further investigated the mode of action of these compounds. Sulfonamides are known to be strong inhibitors of human CAs (20). In *C. elegans*, this class of enzymes is poorly documented. The only documented CA is *cah-4* (25,26). Consequently, we first inventoried CAs in *C. elegans*. A Blast

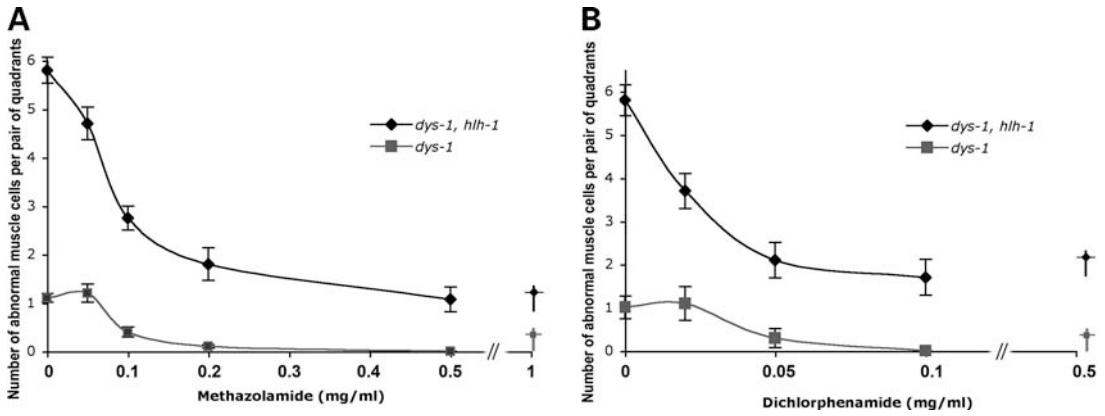

Figure 1. Methazolamide (MTZ) and Dichlorphenamide (DCPM) reduce muscle degeneration in *C. elegans*. Number of missing or degenerating body-wall muscle cells per pair of quadrants of 7-day *dys-1(cx18)*; *hlh-1(cc561)* and *dys-1(cx18)* animals exposed to various concentration of MTZ (**A**) or DCPM (**B**). Abscissa value represents the concentration in mg/ml in the medium. The concentration within the animals is unknown. Standard error of the mean (SEM) is indicated by the vertical lines. Cross symbol (†) represents a toxic concentration (lethality or slow growth).

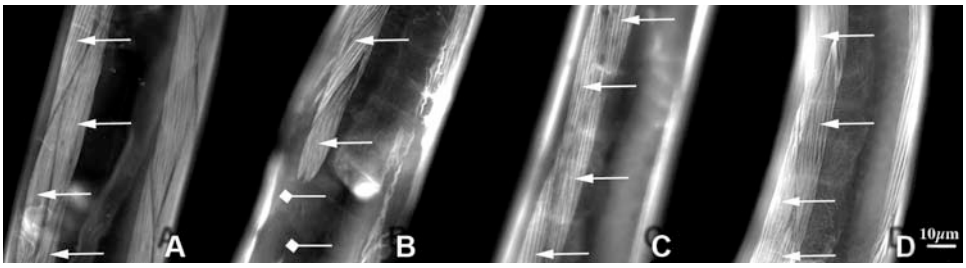

Figure 2. Representative images of muscles of treated and non-treated *C. elegans*. Striated body-wall muscles cells (arrow) of wild-type animal (**A**) and of dystrophic animals *dys-1(cx18)*; *hlh-1(cc561)* treated with DMSO (**B**), MTZ 0.5 mg/ml (2 mM) (**C**) or DCPM 0.1 mg/ml (0.3 mM) (**D**). Body-wall muscles appear as diamond-shaped cells (arrow). Dystrophic animals show a high number of degenerating muscles cells (diamond arrows) rarely seen in animal treated with MTZ or DCPM. These animals were grown 7 days at 15°C in the presence of drugs, and were observed after fixation and phalloidin–rhodamine incubation.

from 14 *Homo sapiens* sequences obtained from the NCBI website revealed six putative CAs in the *C. elegans* genome. These genes are called *cah-1* to *6*. A maximum likelihood tree was constructed (Fig. 4). This tree shows that only *cah-1* and *cah-2* present a high homology with human CA-X and XI. The other worm CAs are too divergent to be matched with human CAs.

We hypothesized that the effect of MTZ and DCPM could be mimicked by knocking down one or several *C. elegans cah* genes. We tested this hypothesis by double-stranded RNA-mediated interference (RNAi) feeding experiments. RNAi is a useful method for gene inactivation in *C. elegans* (27). Four clones available from Geneservice Bank (III-2NO3, II-5LN09, X-7M16, X-6I20) allowed targeting of four of the six *cah* gene (*cah-1*, *cah-2*, *cah-3* and *cah-4*). The last two clones were constructed for the purpose of this study. RNAi experiments with the six clones showed that only inhibition of the gene *cah-4* significantly reduced muscle degeneration in the *dys-1(cx18)*, *hlh-1(cc561)* strain (Fig. 5). RNAi experiments ran on gene combinations did not bring additional information, suggesting that *cah-4* is solely responsible for the drug response to both MTZ and DCPM (Data not shown). Furthermore, *cah-4* RNAi did not impact the activity or growth rate of worms, indicating that it is the *cah-4* reduction *per se* which is responsible for the beneficial effect (Fig. 3A and B). Moreover, this experiment showed a partial restoration of *dys-1*, *hlh-1* locomotion.

Synergy between sulfonamides and CA RNAi in *C. elegans*

To further elucidate the role of these genes in the response of sulfonamide, we tested for a cooperative effect between the presence of sulfonamide and the diminution of each *cah* transcripts. A dose–response experiment was conducted in presence or absence of *cah* dsRNA. No statistical difference was observed between the dose–response control and the dose–response coupled with the inhibition of *cah-1*, *cah-2*, *cah-3*, *cah-5* and *cah-6* transcripts (Fig. 6). The optimal concentration remains around 0.5 mg/ml in all conditions, and the sublethal MTZ concentration remains also unchanged (1 mg/ml). On the contrary, the inhibition of *cah-4* transcripts in presence of MTZ or DCPM showed a dramatic shift of the dose–response curve to the left. The MTZ is lethal at 1 mg/ml in the medium for the negative control and this concentration goes down to 0.1 mg/ml when coupled with an inhibition of *cah-4* transcripts. The optimal concentration to reduce degeneration goes down from 0.5 to 0.01 mg/ml when coupled to *cah-4* RNAi. For DCPM, the toxic concentration is shifted from 0.5 to 0.05 mg/ml when coupled with *cah-4* RNAi and the optimal concentration is shifted from 0.1 to 0.005 mg/ml.

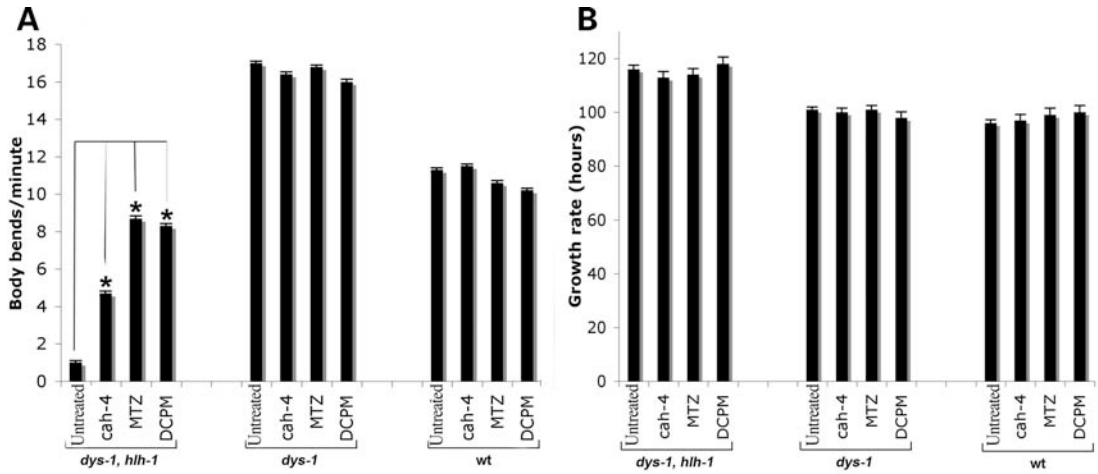

Figure 3. Comparison of locomotion rate and growth rate of MTZ and DCPM treated animals. Locomotion rate (**A**) and growth rate (**B**) of *dys-1(cx18)*; *hlh-1(cc561)*, *dys-1(cx18)* and wild-type adult animals exposed to DMSO 1% (Untreated), *cah-4* RNAi (cah-4), 0.5 mg/ml of MTZ and 0.1 mg/ml of DCPM. Mean of 30 worms ± Standard Error of the Mean (SEM), * different from control at $P < 0.01$.

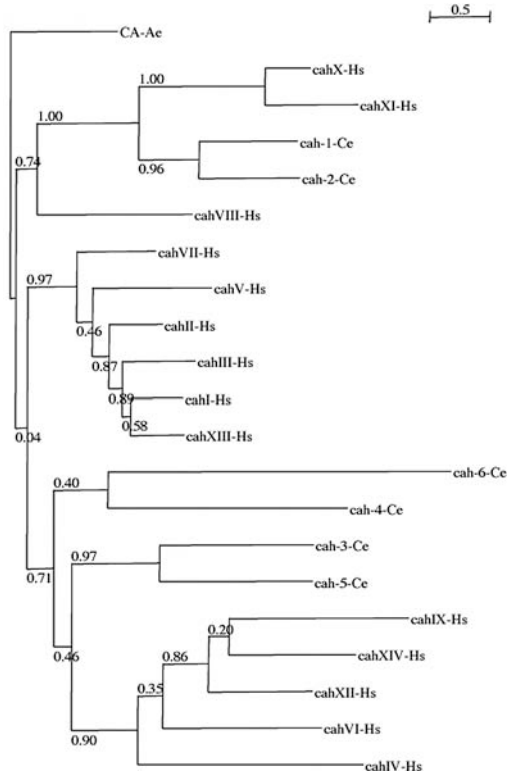

Figure 4. Phylogenetic relationships of *Homo sapiens* (Hs) and putative *C. elegans* (Ce) Carbonic Anhydrase. The tree was constructed by the maximum likelihood method. The number at each node represents bootstrap values from 500 replicates. The *Anthopleura elegantissima* (Ae) CA was used as an outgroup. The bar indicates the number of substitutions per site.

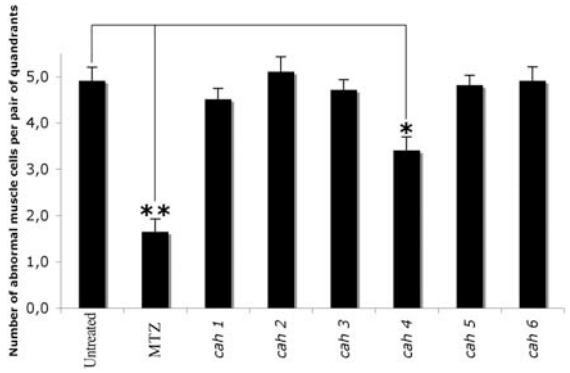

Figure 5. Effect of *cah* gene inhibition on *C. elegans* muscle degeneration. Number of missing or degenerating body-wall muscle cells per pair of quadrants of 7-day *dys-1(cx18)*; *hlh-1(cc561)* animals. Each of the six *C. elegans cah* genes was specifically inhibited by RNAi. Untreated: Dystrophic animals exposed to DMSO 1% and empty vector L4440. MTZ: Dystrophic animals exposed to 0.5 mg/ml of MTZ and empty vector L4440. Mean of 30 worms ± SEM, * different from negative control at $P < 0.05$, ** $P < 0.001$.

These results suggest that the mechanism involved is common to both compounds, and further demonstrate that the protein CAH-4 is their target.

As a negative control the same experiments were performed with Imipramine, Nifedipine and Trimipramine. These drugs have been previously shown to reduce muscle degeneration in *C. elegans* but are not CA inhibitors (28). In presence of *cah-4* dsRNA, their respective sublethal concentration remained unchanged (data not shown), thereby demonstrating that MTZ and DCPM interact with CAH-4 in a specific way.

CAH-4 tissue distributions

We then investigated the tissue expression of *cah-4*. To localize CAH-4, a plasmid carrying the putative endogenous promoter of *cah-4* in frame with GFP was constructed and injected in worms. Fifty fluorescent worms (all stages) were analyzed under confocal microscopy. The GFP protein was localized at all stages in the excretory cell, in the nervous system (nerve ring, dorsal and ventral cord and motor neuron commissures), in body wall muscles and in the anal muscles (Fig. 7). This expression pattern is consistent with the effect observed.

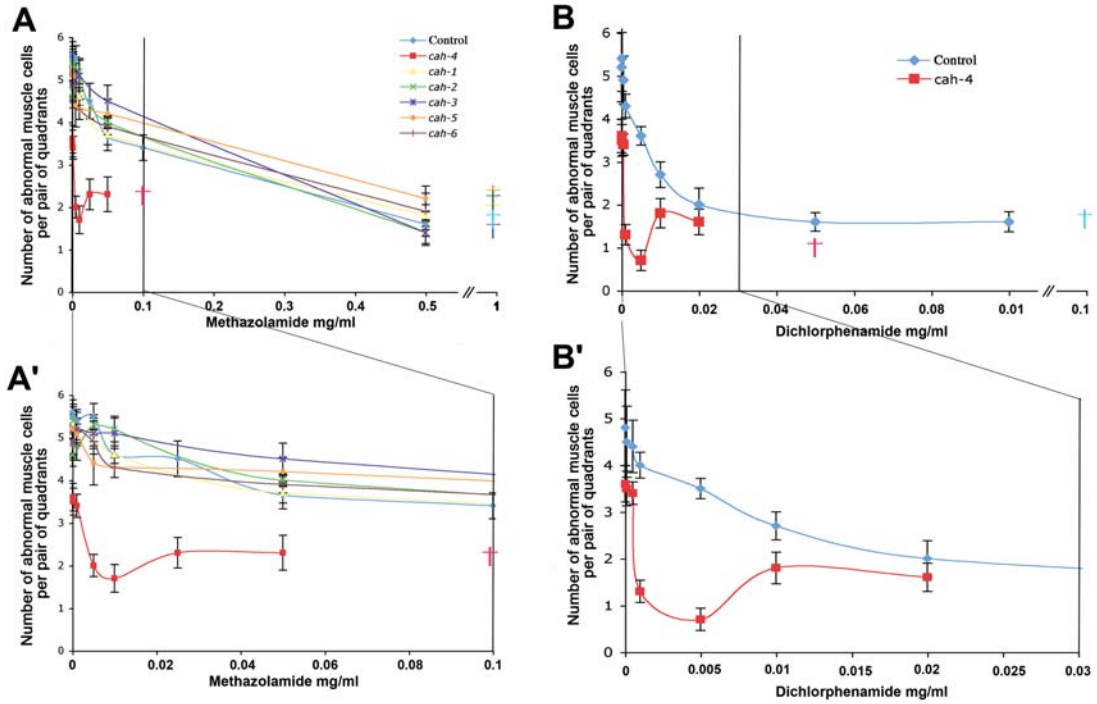

Figure 6. Synergetic effect between sulfonamide treatment and *cah* gene inhibition. Number of missing or degenerating body-wall muscle cells per pair of quadrants of 7-day *dys-1(cx18)*; *hlh-1(cc561)* animals exposed to various concentration of MTZ (A and A′) or DCPM (B and B′) in presence or absence of *cah* dsRNA. Mean of 30 worms ± SEM. Cross symbol (†) represents a toxic concentration.

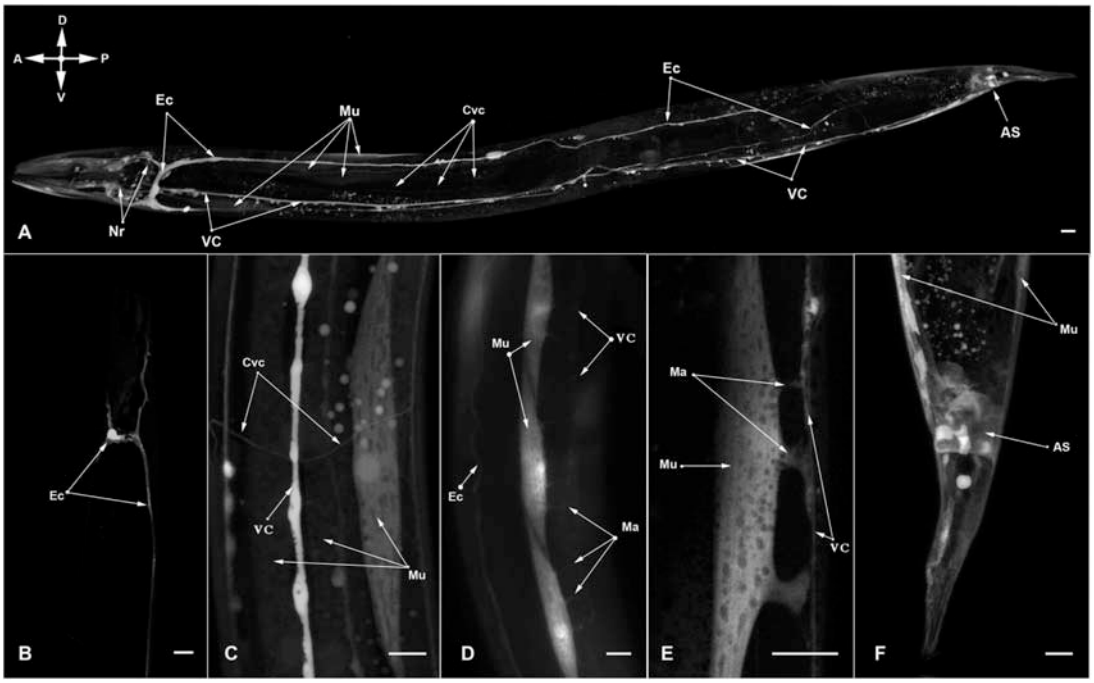

Figure 7. CAH-4 tissue expression. Expression of *cah-4* in *C. elegans* detected by reporter gene. Expression was observed in the excretory cell (Ec), nerve ring (Nr), ventral and dorsal cord (VC, DC), commissure from ventral cord (Cvc), body wall muscle (Mu), muscle arms (Ma) and around the anal sphincter (AS). Auto-fluorescent gut granules are also visible. Bars indicate 10 μM.

Effect of MTZ and DCPM on *mdx* mouse muscle

Treatment of mdx *mice with DCPM and MTZ.* We then analyzed whether MTZ and DCPM would have an effect on the mouse *mdx* model of DMD. Sex- and age-matched (70-day) *mdx* mice were fed 120 days with drug containing food or control food with identical composition, and animals were then analyzed. For DCPM treatment, a low-dose

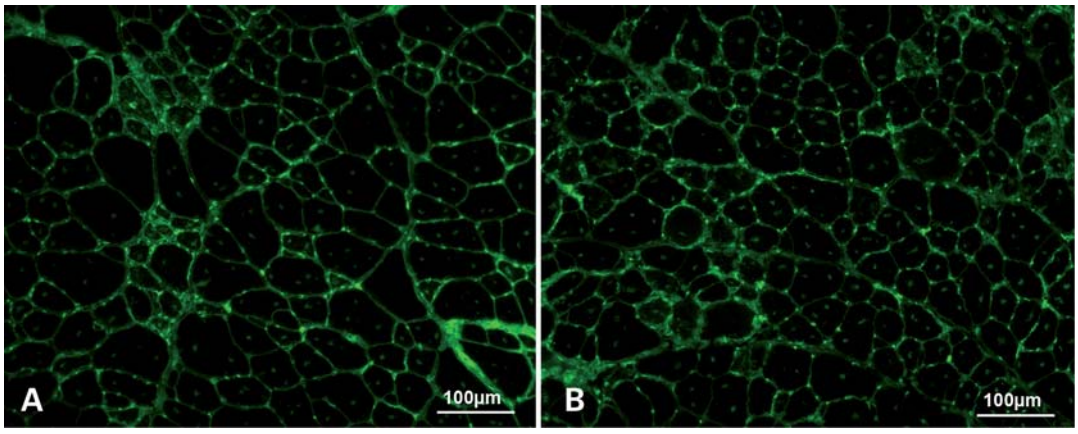

Figure 8. Representative wheat germ agglutinin (WGA) of *tibialis anterior* (TA) muscle. (**A** and **B**) Alexa 488 conjugated WGA-staining of TA muscle of untreated (A) and 5× MTZ-treated (B) *mdx* mice. WGA binds to N-acetylglucosaminyl and sialic acid residues at the border of the muscle fibers.

(15 mg/kg/day) or a high-dose (60 mg/kg/day) was administered, which is, respectively, 5× and 20× human average posology. For MTZ, 20× posology (86 mg/kg/day) was lethal, so we administered a low concentration which was 1× posology (4.3 mg/kg/day) and a high concentration which was 5× posology (21.5 mg/kg/day). Concentrations of drugs in food were calculated on the basis of that *mdx* mice eat ~15% of their body weight per day (L.S., unpublished results). All mice had similar weight at the end of the treatment suggesting that food intake was comparable. Two types of readouts were conducted: histology and force measurement.

Histology assessment of MTZ treated muscles. Muscles from drug-treated animals were histologically analyzed. Representative Wheat Germ Agglutinin (WGA-staining), for *tibialis anterior* (TA) muscles of MTZ high dosage group is shown in Figure 8. We performed Haematoxylin Eosin staining (HE-staining) to obtain a general impression of the histological appearance of both groups to be compared. No obvious differences of the histological appearance became visible for 5× MTZ treated muscles compared with the untreated group (data not shown). However, an automated analysis of the fiber type distribution revealed subtle differences (see below). In Figure 8A and B the Alexa 488 conjugated WGA-staining for sections from untreated and 5× MTZ treated *mdx* mice is shown. The WGA-staining allowed clear delineation of fiber boundaries for determination of minimal fiber diameters. Myosin Heavy Chain (MHC) double staining (Fig. 9A) provided information about the fiber type distribution, MHC isoforms I, and type IIa and IIb fibers, which are separately stained by the protocol applied. Both substances showed no effect on the fiber type composition (data not shown).

Automated histological analysis of muscle sections. In order to obtain a reliable and secured statistical analysis of pathology-relevant histological parameters of dystrophic muscle in *mdx* mice, a standardized and automated quantitative method was developed with S.CO Lifescience (München, Germany) (Fig. 9). Two adequate parameters for analysis of the histological status were chosen. The minimal Feret's diameter of the fibers, and the percentage of centrally nucleated fibers (indicative of muscle regeneration) were determined (29).

Dystrophic muscle typically displays a higher variability of the muscle fiber diameter compared with wild-type muscle. The variance coefficient (VC) of all muscle fiber minimal Feret's diameters of a given muscle cross-section provides a numerical value of the fiber size variability (29). The minimal Feret's diameter is very robust against experimental errors such as the orientation of the sectioning angle. Regarding the second histological parameter, muscles of wild-type mice rarely contain centralized nuclei, whereas muscles of *mdx* mice show an average percentage of up to 66% of centrally nucleated fibers after the first crisis of degeneration and regeneration at around 7 weeks of age.

In this study, we examined about 3000 fibers of TA and diaphragm (DIA) muscles for each 5× MTZ treatment and untreated group covering both parameters. Automated histological analysis was performed only for the 5× MTZ treated group and its untreated control group, because quality of the muscles belonging to the DCPM group was not sufficient and thus analysis not possible.

The histological analysis of the TA muscle showed a significant decrease of the percentage of centrally nucleated fibers in the 5× MTZ treated group (MTZ: 57.4 ± 14.9; control: 65.1 ± 11.2; $P = 0.03$) (Fig. 10A), and a non-significant higher VC with $Z = 487$ in the treatment group compared with $Z = 448$ in the control group ($P > 0.05$). In accordance with the higher VC in the 5× MTZ-treated group, we were able to distinguish a shift of the minimal Feret's diameter towards smaller fibers with diameters <20 µm (Fig. 10C) in the 5× MTZ-treated group ($P = 0.03$), whereas the number of fibers between 30 and 40 µm were higher in the untreated group ($P = 0.02$) (Fig. 10C).

In DIA no significant change in the percentage of centrally nucleated fibers between 5× MTZ treated group (72.1 ± 6.7) and untreated control group (75.1 ± 7.0) was observed ($P = 0.085$) (Fig. 10B) and the VC of the muscle fiber size distribution in diaphragm was slightly lower with $Z = 425$ in the treatment group compared with $Z = 439$ in the untreated group ($P > 0.05$). Moreover, a very similar fiber size distribution was observed in both groups (Fig. 10D).

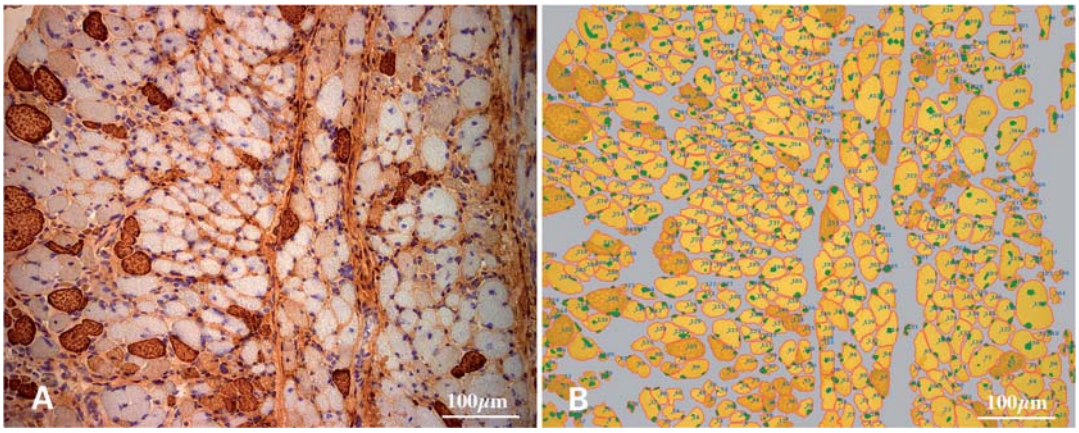

Figure 9. Automated quantitative analysis of muscle histology. (**A**) Original photo of a diaphragm (DIA) section stained with Myosin Heavy Chain (MHC)-double staining of *mdx* mouse. Brown fibers display MHC fiber type I and blue fibers fiber type IIA or IIB. (**B**) Processed photo of the same DIA section mentioned in (**A**). The yellow areas describe the fibers the program recognizes (type I: dark yellow, type II: bright yellow). Each identified fiber is labeled with a number defining its ID. Connective tissue is not recognized (grey areas). Nuclei are marked with green dots.

Muscle force measurements of mdx *mice treated with MTZ and DCPM*. The ability of therapeutic drugs to improve force generation was determined by isometric force measurement using different protocols able to distinguish between maximal force generation capability (tetanic force) and resistance to eccentric contraction. Treatment of mice with DCPM (20× posology) increased significantly the tetanic specific force of *extensor digitorum longus* (EDL) muscle by 30% in the treated group (DCPM: 282 ± 64; untreated: 198 ± 53; $P = 0.034$) (Fig. 11B). This improvement in muscle force generation was not seen in the second treatment group at lower concentration (data not shown).

We further examined in *mdx* EDL muscle the maximal force generation using an eccentric contraction protocol with elongation of the muscle for 10% of its resting length (Lo). Treatment with DCPM at both concentrations, however, was not able to improve this parameter. On the contrary, results in Figure 11A show a significant ($P = 0.034$) higher percentage of the mean force drop in DCPM treated mice ($67 \pm 14\%$) compared with untreated *mdx* mice ($46 \pm 15\%$). These results show that DCPM treatment improved the effective muscle strength, but was not able to increase muscle fiber resistance to exercise.

The 5× MTZ treatment group displayed a non-significant higher percentage of the mean force drop (55 ± 17 versus $49 \pm 15\%$ in the untreated group) (Fig. 11C), whereas tetanic specific force increased in the 5× MTZ treated mice by 25% (MTZ: 264 ± 57; untreated: 197 ± 86; $P = 0.05$), as shown in Figure 11D.

Overall, with the exception of the eccentric contraction test, these substances show a clear improvement of the dystrophic phenotype in *mdx* mice.

DISCUSSION

Caenorhabditis elegans as a model for drug discovery

Our findings confirm the use of *C. elegans* as a model organism for screening, identifying and characterizing potential lead pharmacological agents. In this study, we show the therapeutic potential of a previously unsuspected class of molecules for the treatment of DMD. One of the concerns of using the *C. elegans* model for drug discovery is the determination of the effective dose for a lead compound. The molecules used in this study were provided to the worms through the media. *C. elegans* has an outer exoskeleton (cuticle) which provides protection from environmental chemicals (30). Thus, the effective concentration absorbed through the cuticle and/or the intestinal lumen is not known and is approximately 100–1000× lower than in the medium (28). However, this limitation does not impede the use of *C. elegans*. Data have to be considered mostly in a qualitative manner.

Sulfonamide and CA in *C. elegans*

Sulfonamide is known to be strong inhibitors of several CA in humans (20). After identifying CAs in the worm, we knocked down their expression by RNAi experiments and we found that RNAi inhibition of *cah-4* reduced muscle degeneration (Fig. 4). Since *cah-4* reduction mimics the effect of sulfonamide treatment, it is likely that it is the target of the compounds (Fig. 5). Moreover, several sulfonamides including MTZ and DCPM have already been found to be active on CAH-4 with k_i values at 42 and 38 nM, respectively (25), and null mutants *cah-4(tm2805)* are lethal. We postulated that this lethality is due to the absence of CAH-4 activity since we could mimic it with a high concentration of MTZ (1 mg/ml) or DCPM (0.5 mg/ml). Furthermore, worms display an increased sensitivity to MTZ and DCPM when these treatments are coupled with *cah-4* RNAi (Fig. 6). All together, these results suggest that the gain obtained in the *C. elegans* dystrophin-deficient model is due to an inhibition of CAH-4 activity by sulfonamide.

Furthermore, the *cah-4*::GFP reporter gene was localized in body wall muscles and in the nervous system. Although it cannot be formally demonstrated, it is likely that sulfonamides act directly on muscles for the following reasons: (i) Compounds did not reduce locomotion of *dys-1* and wild-type worms, indicating an absence of a major effect on the

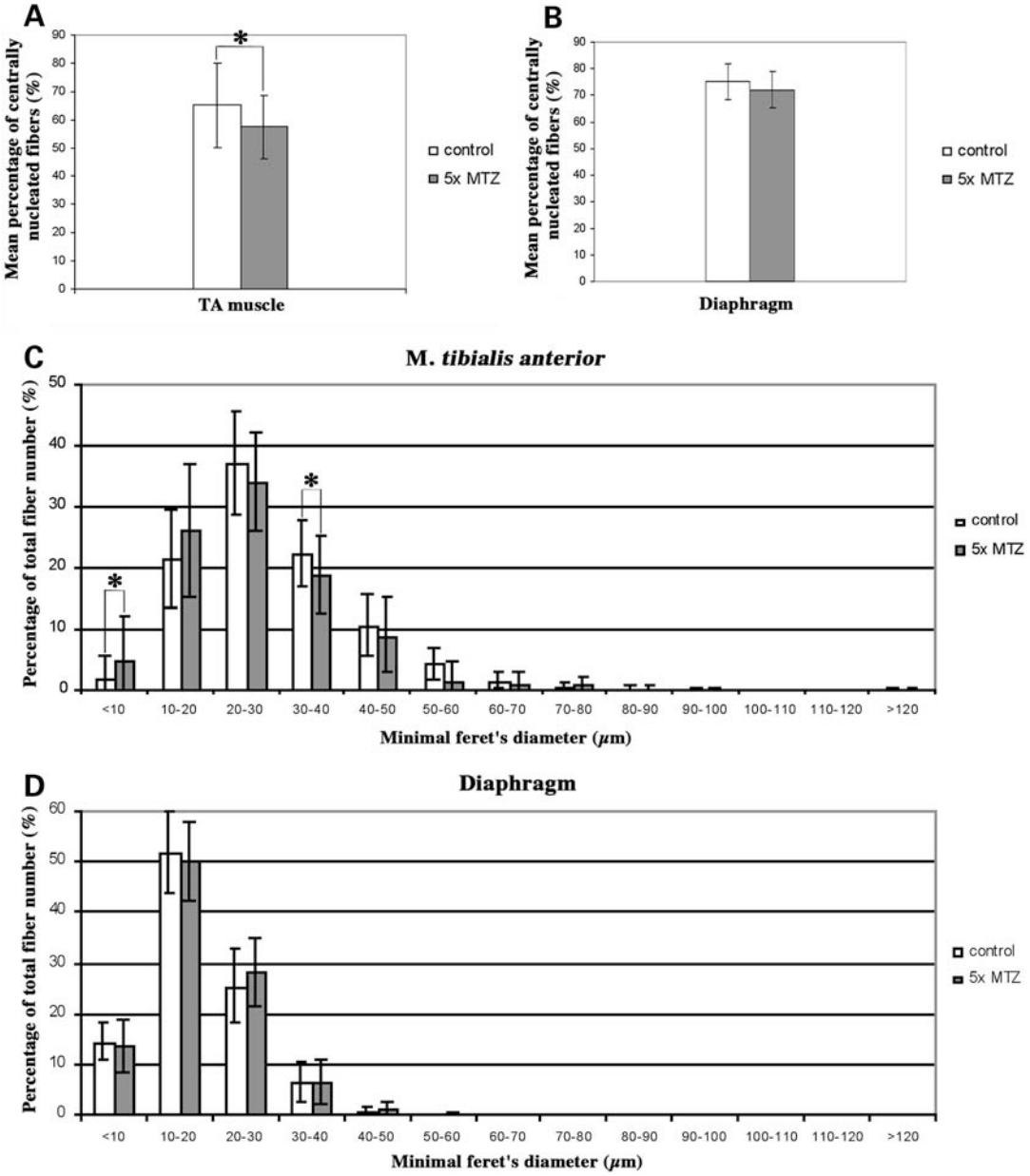

Figure 10. Quantitative assessment of muscle histology. (**A** and **B**) Percentage of centrally nucleated fibers in TA muscle (A) and diaphragm (B) of untreated versus 5× MTZ-treated *mdx* mice. Data expressed as mean ± SD; mean percentage of centrally nucleated fibers ($n = 3000$). (**C** and **D**) Fiber size distribution in TA muscle (C) and DIA (D) of untreated versus 5× MTZ-treated *mdx* mice. * Different from control at $P < 0.05$.

central nervous system (Fig. 3A). (ii) RNAi is poorly active on the nervous system of *C. elegans* (31), yet it is of considerable effect in our experiment.

MTZ and DCPM are known to induce metabolic acidosis and their mechanisms of action most likely involve changes of pH that alter the transmembrane potential and excitability (32). Lower pH values reduce potassium conductance of the cell membrane and have an effect on the activation and inactivation of sodium and calcium channels, respectively (33). On the other hand, acidification of the sarcoplasmic reticulum *trans*-chamber induced a reduction of the unitary conductance of the Ca^{2+} release channel (34). Since we found that calcium channel activity is a critical factor in the progression of dystrophin-dependent muscle degeneration in *C. elegans* (35), we hypothesize that an appropriate concentration of MTZ or DCPM could reduce Ca^{2+} transients and thus decrease muscle degeneration in *C. elegans*.

Effect of MTZ and DCPM on *mdx* mouse muscle

Despite the fact that muscle pathology for dystrophin-deficiency differs between the *mdx* mouse model and human patients, the *mdx* mouse model is the most important animal model for preclinical studies in DMD research (36,37). In the present study, we have applied recommended methods for pre-clinical analysis in DMD research. Readout parameters

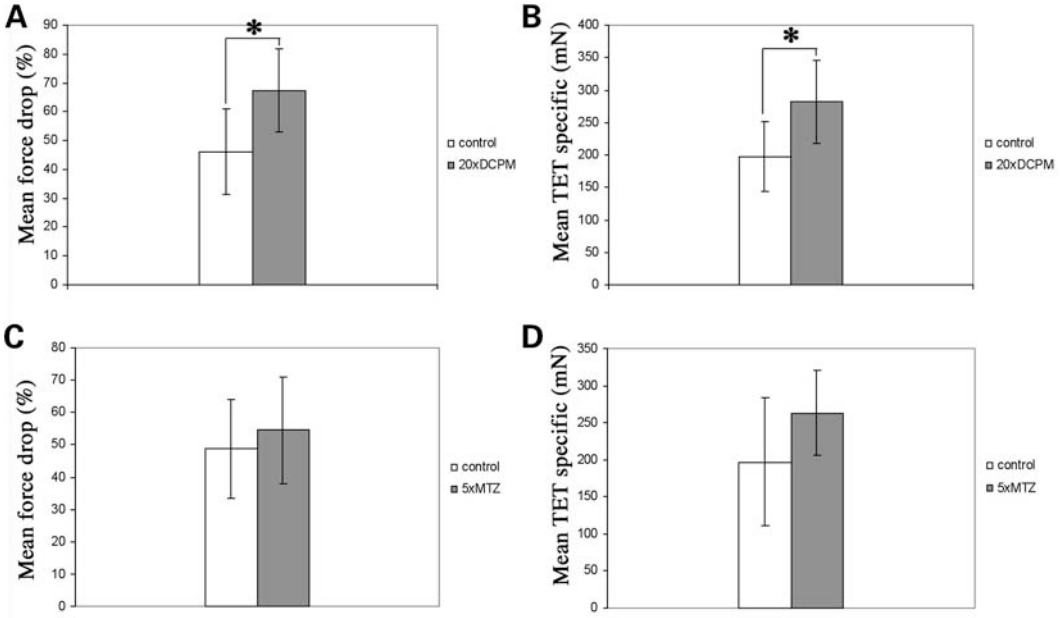

Figure 11. Muscle force measurements of EDL from treated and untreated *mdx* mice. (**A** and **B**) Muscle force measurements for right EDL after 120 days treatment with 20× DCPM of 6-month-old male *mdx* mice ($n_{control} = 7$, $n_{DCPM} = 6$). (A) Mean force drop after eccentric stimulation (B) Mean tetanic specific force (TET specific) obtained by normalization of tetanic maximal force (TET max) with CSA (cross sectional area). (**C** and **D**) Muscle force measurements for EDL after 120 days treatment with 5× MTZ of 6-month-old female *mdx* mice ($n_{control} = 6$, $n_{MTZ} = 5$). (C) Mean force drop after eccentric stimulation of untreated and 5× MTZ-treated *mdx* mice (D) Mean TET specific obtained by normalization of TET max with CSA ($P = 0.05$). Data expressed as mean ± SD. *Different from control at $P < 0.05$.

included muscle force measurement on isolated muscle, and the histological examination including the percentage of centrally nucleated fibers and the VC of the fiber size which reflects the degeneration and regeneration processes.

Histological analysis of the TA muscle revealed a statistically significant decrease in the percentage of centrally nucleated fibers for 5× MTZ treated mice, implying less degeneration/regeneration occurring during the treatment period. This result is particularly remarkable, since the treatment was initiated at an age of 70 days, a time point where intense degenerative and regenerative activity had already taken place (38–40).

Moreover, automated histological analysis revealed an increase in fiber size variability in the 5× MTZ-treatment group, which is not obvious by simple visual inspection of the corresponding HE sections. A detailed analysis of the fiber size distribution revealed the occurrence of more smaller and larger fibers, which typically arise during cycles of regeneration and degeneration, in this group. In addition Neural Cell Adhesion Molecule (NCAM) staining for regenerating fibers clearly showed more NCAM positive fibers, corroborating the higher number of small fibers observed here (data not shown). DIA presents the most severely affected muscle in *mdx* mice. In this study treatment of *mdx* mice with 5× MTZ did not ameliorate the histological parameters of the diaphragm. Possibly, damage associated with dystrophin-deficiency in the diaphragm is too severe to be alleviated by the treatment applied in this study. Also, the treatment window used here may occur to late to show any improvement for the diaphragm.

We then investigated the functional analysis of muscle force measurements of limb muscles. Significant differences between mdx and wild-type mice are easier observed in older mice (41). In the MTZ- and DCPM-high dosage groups an increase of the tetanic specific force led to an improvement of the maximal force. The increase in muscle force was not due to differences in muscle weight or size, since normalization of isolated muscles regarding to these two parameters occurred. The maximal force generation, but not the overall resistance of the muscle to a stimulated endurance protocol, was increased.

A possible mode of action of MTZ and DCPM could be through a reduction of reactive oxygen species, in particular by blocking the muscle-abundant CAIII (42–44). However, since CAIII is more than 10 000 times less sensitive to MTZ compared with other CA isoforms, this hypothesis is still a matter for conjecture (26).

Wetzel *et al*. analyzed the effects of CA inhibitors on muscle force generation and Ca^{2+}-transients. Inhibition of a sarcoplasmatic reticulum CA (SR-CA) isoform was suggested. Indeed, MTZ was shown to be a strong inhibitor of the membrane bound CAIX and of the *C. elegans cah-4*, too, and it was stated that inhibition of only one SR-CA isoform does not affect muscle contraction, whereas inhibition of all three CAs IV, IX and XIV does (26,45). Thus inhibition of these CA isoforms could be implicated in the observed phenotypes in this study as well. Treatment of isolated muscle bundles with one particular inhibitor L-645151 or 6-ethoxyzolamide increased the peak force signals of twitches on EDL and Soleus and showed a prolonged $T^{1/2}$ relaxation time. The authors suggested that CAs generate H^+ outside the SR and supply the ions for the coupled Ca^{2+}–H^+ bidirectional transport across the SR membrane and buffer incoming H^+ ions

inside the SR by catalysis of the reverse reaction (46). Bruns *et al*. (47) showed an acceleration of the $CO_2-HCO_3^-$ reaction of ~1000-fold by the SR-CA. Catalysis by CAII reduced the half time from 7 s to ~7 ms. Inhibition of CAs by sulfonamides was shown to slow Ca^{2+} release from the SR. Consequently, release and uptake of Ca^{2+} as well as the rise time of twitches (increase in force) were prolonged, providing a plausible explanation for the increase in maximal tetanic force by CA inhibitors.

Despite a decrease in resistance of muscle fibers to eccentric contractions, the analyzed substances DCPM and MTZ showed efficacy in the *mdx* mouse and increased the specific tetanic muscle force, demonstrating that a *C. elegans* screen coupled with a mouse model validation strategy can conduct to the identification and characterization of potentials drugs against rare diseases. Differences in CA usage and model physiology likely account for differences of responses observed between the two models.

At this time, sulfonamide like MTZ and DCPM may not be pursued in further preclinical for treatment of DMD, but the development of isozyme-specific or at least organ-selective CA inhibitors may be highly beneficial to improve their efficacy against DMD and applied to other muscular dystrophies, as well as devoid of major side effects.

MATERIALS AND METHODS

Strains and culture conditions

Caenorhabditis elegans strains were cultured at 15°C on 6 cm Petri dishes containing NGM agar and a lawn of *Escherichia coli* OP50 unless stated otherwise. The *dys-1(cx18)*; *hlh-1(cc561)* strain was grown at 15°C, which is the permissive temperature for the ts mutation *hlh-1(cc561)* (17). The wild-type N2 strain was obtained from the *Caenorhabditis* Genetics Center.

Pharmacological compounds

All pharmacological compounds were obtained from Sigma Chemical Co. (St. Louis, MO, USA). Concentrated solutions of each drug were prepared by dissolving compounds in DMSO. *C. elegans* tolerates DMSO up to a final concentration of 2% vol/vol. Compounds were added to liquid NGM that had been autoclaved and cooled to 55°C, and the media was immediately mixed and dispensed into Petri dishes. *C. elegans* are permeable to aqueous and organic molecules, although the tough, outer cuticle may necessitate high concentrations. It is admitted that drugs penetrate the animals both by diffusion through the cuticle and ingestion (37). Drugs used in this study were: MTZ, DCPM.

Muscle observation and analysis on *C. elegans*

The body wall muscles of *C. elegans* are divided into four quadrants (ventral right and left, dorsal right and left) each of which consists of 23 or 24 trapezoidal cells, arranged in two staggered rows. Muscle observation was performed on 7-day animals, after fixation, by rhodamine coupled-phalloidin staining, a marker of filamentous actin. Staining was done according to Waterston *et al*. (48). Slides were observed on a Zeiss Axioplan microscope. A body wall muscle cell is considered degenerating when its actin fibers are fragmented or destroyed (17) (Fig. 1). Only the two most visible muscle quadrants of each animal were scored. Numbers were compared by a Student's *t*-test.

Locomotion rate and growth rate

To estimate the locomotion rate of worms, 7-day animals were scored for the number of body bends generated during an interval of 1 min. A body bend was defined as one complete sinusoidal movement from maximum to minimum amplitude and back again. The growth rate refers to the time from P0 egg to the first F1 egg (generation time). At last 30 worms were examined.

Phylogenetic analyses

To search for CA in *C. elegans*, a Blastp search was performed on *Caenorhabditis elegans* genome (taxid: 6239) with 14 Homo sapiens CAs sequences obtained from the NCBI website as query sequence. CA1 (NP_001729.1), CA2 (NP_000058.1), CA3 (AAH04897.1), CA4 (NP_000708.1), CA5 (NP_001730.1), CA6 (EAW71606.1), CA 7 (EAW83046.1), CA8 (NP_004047.3), CA9 (NP_001207.2), CA10 (NP_064563.1), CA11 (NP_001208.2), CA12 (EAW77648.1), CA13 (NP_940986.1) and CA14 (NP_036245.1). The *C. elegans* sequences selected are: *cah-1* (NP_498083.1), *cah-2* (NP_495567.3), *cah-3* (NP_510674.1), *cah-4* (NP_510265.1), *cah-5* (NP_509186.3) and *cah-6* (NP_491189.1). A maximum likelihood tree was constructed with SEEVIEW version 4.0 (49), based on alignment using MUSCLE (MUltiple Sequence Comparison by Log-Expectation) (50). The *Anthopleura elegantissima CA* sequence (AF140537_1) was used as an out-group. The bootstrap was performed with 500 replicates.

RNAi procedure

RNAi experiments was performed on NGM plates supplemented with 100 μg/ml ampicillin, 12.5 μg/ml tetracycline and 1 mM IPTG as previously described (51). The RNAi clones for *cah*-1, *cah-2*, *cah-3* and *cah-4* were obtained from the Geneservice library. RNAi for *cah-5* and *cah-6* were obtained by amplification of ~600 bp of genomic DNA of either gene and cloned into the RNAi feeding vectors L4440 (Courtesy of Dr Andrew Fire). Bacterial suspensions were used to seed RNAi plates. Five adult gravid worms were put on plate for one night and removed, so as the progeny were exposed to drug and RNAi from hatching to fixation. All animals were fixed and observed at day 7. As a control, *pos-1* RNAi knockdown performed in parallel resulted in near 100% embryonic lethality.

Generation of *cah-4*::GFP construct and localization

The putative endogenous promoter of the *cah-4* gene has been cloned in-frame with GFP in pPD95.67 (provided by A. Fire). To ensure the amplification of *cah-4* promoter region, ~3 kb

upstream of the second ATG start codon of *cah-4* have been amplified. Hermaphrodite from *dpy-5*(e907) strain (CB907) injected with 150 ng/μl pCeh361 (dpy-5 rescuing construct), 10 ng/μl of promoter-*cah-4*::GFP fusion PCR product. Plasmid microinjection was performed as described (52). Individual F1 wild-types were isolated and we retained a line that transmitted F2 transgenics. Transgenic worms with GFP fluorescence were selected, and the animals were viewed by fluorescence microscopy on a Zeiss LSM 510 Meta fluorescence confocal microscope.

Mice and treatment

mdx mice were obtained from Charles River Laboratories, Belgium. All experiments were conducted in accordance with the guidelines of the institutional animal care committee.

Feeding started at an age of 70 days for mice with both 20× (60 mg/kg/day) and 5× (15 mg/kg/day) posology DCPM and 5× (21.5 mg/kg/day) and 1× (4.3 mg/kg/day) posology MTZ containing food. Control food consisted of the same compounds as the experimental food except the effective substances and did not show any effect on the weight, health and behavior of the mice.

Muscle force measurement

After feeding for 120 days *Musculus extensor digitorum longus* was removed and connected to an isometric force transducer (type GRA FT-03; FMI, Seeheim, Germany) (model MIO-0501 DC-Brückenmeßverstärker; ALFOS AG, Biel-Benken; FMI, Seeheim, Germany) coupled to a signal amplifier (model MIO-0501 DC-Brückenmeßverstärker; FMI, Seeheim, Germany). Electrical field stimulation was generated by means of platinum electrodes on both sides of the muscle. Supramaximal stimuli with monophasic pulse duration of 1 ms were released through a computer-controlled electrical stimulator (model ISG-8834/1-S: FMI, Seeheim, Germany). Maximal isometric twitch force was assessed by three twitch stimulations. The maximal isometric tetanic force was measured stimulating the muscle at 125 Hz for 175 ms. Specific force was obtained by normalizing maximum tetanic force on total muscle cross-sectional area (CSA). CSA was calculated by following formula (53):

$$\frac{\text{muscle mass[mg]}}{\text{fiber length[mm]}*1.06\text{mg/mm}}.$$

Measurements for eccentric contraction were performed in principle as described (54).

Histochemistry and immunohistochemistry

Eight-micrometer serial cross sections of *M. tibialis anterior* and diaphragm were stained with Haematoxylin–Eosin and sequentially with antibodies against type I myosin heavy chain and type II (IIa and IIb) myosin heavy chain for MHC-double staining, respectively. HE-staining was carried out according to standard protocols. The antibody against type I myosin heavy chain (NovoCastra, Newcastle upon Tyne, UK) was diluted 1 : 100 as well as the type II myosin heavy chain antibody (NovoCastra, Newcastle upon Tyne, UK). Each incubation of the sections with one of the two primary antibodies was followed by staining with the secondary antibody rabbit anti mouse Ig horseradish peroxidise (DAKO, Glostrop, Denmark) diluted 1 : 100. The different myosin heavy chain fiber types were visualized sequentially by different substrates 3,3′ diaminobenzidine (Sigma-Aldrich, Steinheim, Germany) showing a brown color (type I) and the substrate provided by the Vector SG visualization solution (Vector Laboratories, Burlinhame, USA) showing a blue color (type IIa and IIb). After the first color reaction the sections were blocked with fetal calf serum before the second primary antibody was applied.

The fiber boundaries were stained by 100 ng/ml WGA conjugated to Alexa Fluor 488 (Molecular Probes, Leiden, Netherlands). Nuclei were stained with 10 ng/ml DAPI (Sigma, Steinheim, Germany). Finally, cover slips were mounted in DakoCytomation Fluorescent (DAKO, Glostrop, Denmark).

Quantitative assessment of muscle histology

Automatic quantitative analysis of muscle histology was performed with a special designed module for the image analysis system S.CORE by S.CO LifeScience, Munich, Germany. Three different images of the observed section were taken in parallel: (i) Green fluorescent WGA staining to display the fiber boundaries, (ii) Blue fluorescent DAPI staining to show the nuclei, (iii) MHC-double staining to visualize all fibers which are positive for type I MHC or type IIa and IIb MHC, respectively. In the first image all membrane structures were subtracted from background, leading to a mask for the individual muscle fibers, and the minimal Feret's diameter calculated.

This mask was superimposed first with the DAPI image to quantify the number of nuclei within each single muscle fiber and subsequently with the MHC-double staining to determine the fibers positive for type I MHC or type IIa and IIb MHC, respectively. The VC was calculated using the following formula:

$$Z = 1000^* \frac{\text{S.D. of muscle of fiber min} \cdot \text{Feret's diameter}}{\text{Mean muscle fiber min} \cdot \text{Feret's diameter}}.$$

Automated histological analysis was performed only for the 5× MTZ treated group and the corresponding control group, because the quality of the muscles belonging to the DCPM group was not sufficient for analysis.

Statistical analysis

Statistical analysis was performed using SPSS Statistics 17.0 software (SPSS GmbH Software, Munich, Germany). All data sets were tested for normal distribution using the Kolmogorov–Smirnov test. Those data subsets that showed a normal distribution were analyzed performing a *t*-test. All others were tested with the Mann–Whitney test.

ACKNOWLEDGEMENTS

We thank the *C. elegans* Genetics Center for providing strains. We thank Kathrin Gieseler for expert opinion and Ursula

Klutzny and Anja Pertl for excellent technical support, Dana Matzek for fosterage of our mice. Finally, we want to thank Dr Markus Eblenkamp and his S.CO Lifescience team for developing and performing the automated histological analysis.

Conflict of Interest statement. None declared.

FUNDING

This work was supported by the Association Française contre les Myopathies (AFM) and by the European Muscle Development Network (MYORES). The work integrated into an individual research project within the MD-NET funded by the German ministry of education and research (BMBF, Bonn, Germany).

REFERENCES

1. Kunkel, L.M., Monaco, A.P., Bertelson, C.J. and Colletti, C.A. (1986) Molecular genetics of Duchenne muscular dystrophy. *Cold Spring Harb. Symp. Quant. Biol.*, **51**, 349–351.
2. Koenig, M., Hoffman, E.P., Bertelson, C.J., Monaco, A.P., Feener, C. and Kunkel, L.M. (1987) Complete cloning of the Duchenne muscular dystrophy (DMD) cDNA and preliminary genomic organization of the DMD gene in normal and affected individuals. *Cell*, **50**, 509–517.
3. Rando, T.A. (2001) The dystrophin-glycoprotein complex, cellular signaling, and the regulation of cell survival in the muscular dystrophies. *Muscle Nerve*, **24**, 1575–1594.
4. Rentschler, S., Linn, H., Deininger, K., Bedford, M.T., Espanel, X. and Sudol, M. (1999) The WW domain of dystrophin requires EF-hands region to interact with beta-dystroglycan. *Biol. Chem.*, **380**, 431–442.
5. Campbell, K.P. and Kahl, S.D. (1989) Association of dystrophin and an integral membrane glycoprotein. *Nature*, **338**, 259–262.
6. Wells, D.J. (2008) Treatments for muscular dystrophy, increased treatment options for Duchenne and related muscular dystropies. *Gene Ther.*, **15**, 1077–1078.
7. Manzur, A.Y., Kuntzer, T., Pike, M. and Swan, A. (2004) Glucocorticoid corticosteroids for Duchenne muscular dystrophy. *Cochrane Database Syst. Rev.*, **2**, CD003725.
8. Rodino-Klapac, L.R., Chicoine, L.G., Kaspar, B.K. and Mendell, J.R. (2007) Gene therapy for duchenne muscular dystrophy, expectations and challenges. *Arch. Neurol.*, **64**, 1236–1241.
9. Wilton, S.D. and Fletcher, S. (2005) Antisense oligonucleotides in the treatment of Duchenne muscular dystrophy, Where are we now? *Neuromuscul. Disord.*, **15**, 399–402.
10. Miura, P. and Jasmin, B.J. (2006) Utrophin upregulation for treating Duchenne or Becker muscular dystrophy, how close are we? *Trends Mol. Med.*, **12**, 122–129.
11. Cossu, G. and Sampaolesi, M. (2007) New therapies for Duchenne muscular dystrophy, challenges, prospects and clinical trials. *Trends Mol. Med.*, **13**, 520–526.
12. Grounds, M.D., Radley, H.G., Lynch, G.S., Nagaraju, K. and De Luca, A. (2008) Towards developing standard operating procedures for pre-clinical testing in the *mdx* mouse model of Duchenne muscular dystrophy. *Neurobiol. Dis.*, **31**, 1–19.
13. Kaletta, T. and Hengartner, M.O. (2006) Finding function in novel targets, *C. elegans* as a model organism. *Nat. Rev. Drug Discov.*, **5**, 387–398.
14. Segalat, L. (2007) Invertebrate animal models of diseases as screening tools in drug discovery. *ACS Chem. Biol.*, **2**, 231–236.
15. Nass, R., Merchant, K.M. and Ryan, T. (2008) *Caenohabditis elegans* in Parkinson's disease drug discovery, addressing an unmet medical need. *Mol. Interv.*, **8**, 284–293.
16. Bessou, C., Giugia, J.B., Franks, C.J., Holden-Dye, L. and Segalat, L. (1998) Mutations in the *Caenorhabditis elegans* dystrophin-like gene *dys-1* lead to hyperactivity and suggest a link with cholinergic transmission. *Neurogenetics*, **2**, 61–72.
17. Gieseler, K., Grisoni, K. and Segalat, L. (2000) Genetic suppression of phenotypes arising from mutations in dystrophin-related genes in *Caenorhabditis elegans*. *Curr. Biol.*, **10**, 1092–1097.
18. Moerman, D.G. and Williams, B.D. (2006) Sarcomere assembly in *C. elegans* muscle. *WormBook*, 1–16.
19. Lindskog, S. (1997) Structure and mechanism of carbonic anhydrase. *Pharmacol. Ther.*, **74**, 1–20.
20. Supuran, C.T., Scozzafava, A. and Casini, A. (2003) Carbonic anhydrase inhibitors. *Med. Res. Rev.*, **23**, 146–189.
21. Pastorekova, S., Parkkila, S., Pastorek, J. and Supuran, C.T. (2004) Carbonic anhydrases, current state of the art, therapeutic applications and future prospects. *J. Enzyme Inhib. Med. Chem.*, **19**, 199–229.
22. Hewett-Emmett, D. (2000) Evolution and distribution of the carbonic anhydrase gene families. *EXS*, **90**, 29–76.
23. Supuran, C.T. and Scozzafava, A. (2000) Activation of carbonic anhydrase isozymes. *EXS*, **90**, 197–219.
24. Gaud, A., Simon, J.M., Witzel, T., Carre-Pierrat, M., Wermuth, C.G. and Segalat, L. (2004) Prednisone reduces muscle degeneration in dystrophin-deficient *Caenorhabditis elegans*. *Neuromuscul. Disord.*, **14**, 365–370.
25. Hall, R.A., Vullo, D., Innocenti, A., Scozzafava, A., Supuran, C.T., Klappa, P. and Muhlschlegel, F.A. (2008) External pH influences the transcriptional profile of the carbonic anhydrase, CAH-4b in *Caenorhabditis elegans*. *Mol. Biochem. Parasitol*, **161**, 140–149.
26. Crocetti, L., Maresca, A., Temperini, C., Hall, R.A., Scozzafava, A., Muhlschlegel, F.A. and Supuran, C.T. (2009) A thiabendazole sulfonamide shows potent inhibitory activity against mammalian and nematode alpha-carbonic anhydrases. *Bioorg. Med. Chem. Lett.*, **19**, 1371–1375.
27. Fire, A., Xu, S., Montgomery, M.K., Kostas, S.A., Driver, S.E. and Mello, C.C. (1998) Potent and specific genetic interference by double-stranded RNA in *Caenorhabditis elegans*. *Nature*, **391**, 806–811.
28. Carre-Pierrat, M., Mariol, M.C., Chambonnier, L., Laugraud, A., Heskia, F., Giacomotto, J. and Segalat, L. (2006) Blocking of striated muscle degeneration by serotonin in *C. elegans*. *J. Muscle Res. Cell Motil.*, **27**, 253–258.
29. Briguet, A., Courdier-Fruh, I., Foster, M., Meier, T. and Magyar, J.P. (2004) Histological parameters for the quantitative assessment of muscular dystrophy in the *mdx*-mouse. *Neuromuscul. Disord.*, **14**, 675–682.
30. Page, A.P. and Johnstone, I.L. (2007) The cuticle. *WormBook*, 1–15.
31. Kennedy, S., Wang, D. and Ruvkun, G. (2004) A conserved siRNA-degrading RNase negatively regulates RNA interference in *C. elegans*. *Nature*, **427**, 645–649.
32. Spacey, S.D., Hildebrand, M.E., Materek, L.A., Bird, T.D. and Snutch, T.P. (2004) Functional implications of a novel EA2 mutation in the P/Q-type calcium channel. *Ann. Neurol.*, **56**, 213–220.
33. Shapiro, M.S., Gomeza, J., Hamilton, S.E., Hille, B., Loose, M.D., Nathanson, N.M., Roche, J.P. and Wess, J. (2001) Identification of subtypes of muscarinic receptors that regulate Ca^{2+} and K^{+} channel activity in sympathetic neurons. *Life Sci.*, **68**, 2481–2487.
34. Rousseau, E. and Pinkos, J. (1990) pH modulates conducting and gating behaviour of single calcium release channels. *Pflugers Arch.*, **415**, 645–647.
35. Mariol, M.C. and Segalat, L. (2001) Muscular degeneration in the absence of dystrophin is a calcium-dependent process. *Curr. Biol.*, **11**, 1691–1694.
36. Willmann, R., Possekel, S., Dubach-Powell, J., Meier, T. and Ruegg, M.A. (2009) Mammalian animal models for Duchenne muscular dystrophy. *Neuromuscul. Disord.*, **19**, 241–249.
37. Spurney, C.F., Gordish-Dressman, H., Guerron, A.D., Sali, A., Pandey, G.S., Rawat, R., Van Der Meulen, J.H., Cha, H.J., Pistilli, E.E., Partridge, T.A. *et al.* (2009) Preclinical drug trials in the *mdx* mouse, assessment of reliable and sensitive outcome measures. *Muscle Nerve*, **39**, 591–602.
38. Carnwath, J.W. and Shotton, D.M. (1987) Muscular dystrophy in the *mdx* mouse, histopathology of the soleus and extensor digitorum longus muscles. *J. Neurol. Sci.*, **80**, 39–54.
39. Coulton, G.R., Morgan, J.E., Partridge, T.A. and Sloper, J.C. (1988) The mdx mouse skeletal muscle myopathy, I. A histological, morphometric and biochemical investigation. *Neuropathol. Appl. Neurobiol.*, **14**, 53–70.
40. Torres, L.F. and Duchen, L.W. (1987) The mutant mdx, inherited myopathy in the mouse. Morphological studies of nerves, muscles and end-plates. *Brain*, **110**, 269–299.

41. Dunant, P., Larochelle, N., Thirion, C., Stucka, R., Ursu, D., Petrof, B.J., Wolf, E. and Lochmuller, H. (2003) Expression of dystrophin driven by the 1.35-kb MCK promoter ameliorates muscular dystrophy in fast, but not in slow muscles of transgenic mdx mice. *Mol. Ther.*, **8**, 80–89.
42. McKenna, M.J., Medved, I., Goodman, C.A., Brown, M.J., Bjorksten, A.R., Murphy, K.T., Petersen, A.C., Sostaric, S. and Gong, X. (2006) N-acetylcysteine attenuates the decline in muscle Na^+, K^+-pump activity and delays fatigue during prolonged exercise in humans. *J. Physiol.*, **576**, 279–288.
43. Reid, M.B. (2008) Free radicals and muscle fatigue, Of ROS, canaries, and the IOC. *Free Radic. Biol. Med.*, **44**, 169–179.
44. Räisänen, S.R., Lehenkari, P., Tasanen, M., Rahkila, P., Härkonen, P.L. and Väänäen, H.K. (1999) Carbonic anhydrase III protects cells from hydrogen peroxide-induced apoptosis. *FASEB J.*, **13**, 513–522.
45. Scheibe, R.J., Mundhenk, K., Becker, T., Hallerdei, J., Waheed, A., Shah, G.N., Sly, W.S., Gros, G. and Wetzel, P. (2008) Carbonic anhydrase IV and IX, subcellular localization and functional role in mouse skeletal muscle. *Am. J. Physiol. Cell Physiol.*, **294**, 402–412.
46. Wetzel, P., Kleinke, T., Papadopoulos, S. and Gros, G. (2002) Inhibition of muscle carbonic anhydrase slows the Ca(2+) transient in rat skeletal muscle fibers. *Am. J. Physiol. Cell Physiol.*, **283**, C1242–C1253.
47. Bruns, W., Dermietzel, R. and Gros, G. (1986) Carbonic anhydrase in the sarcoplasmic reticulum of rabbit skeletal muscle. *J. Physiol.*, **371**, 351–364.
48. Waterston, R.H., Hirsh, D. and Lane, T.R. (1984) Dominant mutations affecting muscle structure in Caenorhabditis elegans that map near the actin gene cluster. *J. Mol. Biol.*, **180**, 473–496.
49. Galtier, N., Gouy, M. and Gautier, C. (1996) SEAVIEW and PHYLO_WIN, two graphic tools for sequence alignment and molecular phylogeny. *Comput. Appl. Biosci.*, **12**, 543–548.
50. Edgar, R.C. (2004) MUSCLE, multiple sequence alignment with high accuracy and high throughput. *Nucleic Acids Res.*, **32**, 1792–1797.
51. Timmons, L. and Fire, A. (1998) Specific interference by ingested dsRNA. *Nature*, **395**, 854.
52. Mello, C. and Fire, A. (1995) DNA transformation. *Methods Cell. Biol.*, **48**, 451–482.
53. Gorospe, J.R. and Hoffman, E.P. (1992) Duchenne muscular dystrophy. *Curr. Opin. Rheumatol.*, **4**, 794–800.
54. Petrof, B.J., Shrager, J.B., Stedman, H.H., Kelly, A.M. and Sweeney, H.L. (1993) Dystrophin protects the sarcolemma from stresses developed during muscle contraction. *Proc. Natl. Acad. Sci. USA*, **90**, 3710–3714.